Time-Frequency Excision for GNSS Applications

Daniele Borio[1], Laura Camoriano[2], Simone Savasta[1], Letizia Lo Presti[1]

Abstract

Interference detection and mitigation in Global Navigation Satellite Systems (GNSSs) are an important issue for both military and civilian applications. In this paper we propose a novel Time-Frequency algorithm for interference excision in the context of GNSS. The use of Infinite Impulse Response (IIR) notch filters for the interference excision is introduced and analytical formulas for the detection of the disturbing signals are derived.

The proposed method is tested by simulations and compared with past Time-Frequency excision algorithms, proving its effectiveness for interference removal.

Index Terms

Global Navigation Satellite System (GNSS), Interference, Time-Frequency Analysis, Signal Acquisition, Receiver Operative Characteristic (ROC).

I. Introduction

Interference detection and mitigation in the Global Navigation Satellite System (GNSS) context are an important issue for both military and civilian applications. Due to its weakness, the GNSS signal is subject to interferences that are extremely different in terms of time and frequency characteristics [1]. Thus the design of a general mitigator, able to efficiently deal with different kinds of interference is a complex problem. A solution is represented by the Time-Frequency (TF) analysis, that allows to detect and efficiently remove a great variety of disturbing signals.

1) Dipartimento di Elettronica, Politecnico di Torino. Corso Duca degli Abruzzi, 10129 Torino, Italy. Email: name.surname@polito.it.

2) Istituto Superiore Mario Boella. Via Pier Carlo Boggio 61,10138 Torino, Italy. Email: laura.camoriano@ismb.it.

Corresponding author: Daniele Borio. Tel: 0039 0115644053, fax: 0039 0115644099

In the past, a great interest has been devoted to TF excision techniques in the context of Direct-Sequence Spread Spectrum (DSSS) communications [2], [3], [4], [5], [6], [7]. This interest is justified by the fact that the power of DSSS signals is spread over a bandwidth that is much wider than the original information bandwidth. As a result, DSSS signals present power spectral densities that can be completely hidden under the noise floor and consequently they impact only marginally the interference detection/estimation on the TF plane.

TF excision techniques usually rely on the estimation of the interference instantaneous frequency [8]. This information is used to control the coefficients of an excision filter that adaptively removes the disturbing signal [2], [3], [4]. An alternative approach [6] consists in using the instantaneous frequency estimation to down-convert the interference around the zero frequency. A time-invariant high-pass filter is then used to remove the jammer and the original frequency content of the received signal is restored.

A second class of TF excision algorithms is based on the direct interference mitigation on the TF plane [5], [9]: all those samples, belonging to the TF plane, that passes a fixed threshold are removed since considered generated by the interference. An interference-free signal is then synthesized from the mitigated TF representation.

The majority of GNSS, such as Galileo, GPS and the Japanese QZSS, employs DSSS modulations, and thus TF excision techniques can be applied to GNSS receivers as well [9]. However GNSS signals are generally characterized by lower received power and longer spreading codes with respect to the ones used for communication applications. Moreover the bit error rate (BER) represents a secondary aspect since a GNSS receiver has, at first, to detect the satellite presence and to correctly estimate the signal delay and Doppler frequency. All these aspects are not generally considered in the design of TF excision techniques.

This paper deals with the design of a TF excision algorithm for GNSS applications. Our work is a generalization of the technique proposed in [6]. As in [6], we propose an excision algorithm based on three functional blocks: the TF representation, the instantaneous frequency estimation unit and the excision filter. The role of each component is discussed and the performance with respect to these three elements analyzed. The length of the GNSS spreading codes limits the use of computationally complex TF representations and thus the analysis is limited to the spectrogram and to the Wigner-Ville distribution.

A simple algorithm called *peaks-interpolation* is used for estimating the interference instanta-

neous frequency. This algorithm selects the samples of the TF representation that pass a fixed threshold and provides, as instantaneous frequency estimation, the polynomial curve that better interpolates these TF points. The threshold is determined by fixing a false interference detection probability. This kind of approach is new in the context of TF algorithms, in which only empirical rules for the threshold determination are generally used [9][5].

We also consider the use of an Infinite Impulse Response (IIR) filter for the interference excision. In the past literature [6], [3], [4] only Finite Impulse Response (FIR) filters with a low number of coefficients were employed. This choice was usually justified by the fact that a filter with a long impulse response introduces long correlations among the samples of the DSSS signal. These correlations cause self-noise that can reduce the system performance. However adaptive IIR notch filters are commonly used for GNSS interference excision [10], [11], [12]. In fact, due to the low power of the GNSS signal and thanks to long spreading codes, self-noise does not generally represent a threat for GNSS applications. Moreover, longer spreading codes make tolerable a longer correlation between the useful signal samples. In this paper a single-pole notch filter is adopted and the role of the pole contraction factor, that regulates the notch width, is discussed.

Different aspects, not considered in the previous literature, are analyzed, and in particular the performances of the GNSS acquisition block with and without mitigation unit are studied. The acquisition Receiver Operative Characteristics (ROCs) have been adopted as metrics for establishing the effectiveness of the proposed algorithm.

The paper is organized as follows: in Section II the structure of the GNSS signal is reviewed and the acquisition process briefly discussed. Section III describes the excision algorithm, detailing the three different functional blocks. In Section III the principles for the threshold determination are also exposed. The algorithm performances are analyzed in Section IV and a comparison with the technique proposed in [6] is also provided. Finally Section V concludes the paper.

II. Signal and System Model

The input of the acquisition block is generally an IF digital signal obtained at the output of front-end, which can be written in the form [13]:

$$r[n] = r(nT_s) = \sum_{i=1}^{L_s} y_{IF,i}(nT_s) + N_{IF}(nT_s) \tag{1}$$

where L_s is the number of satellites in view, T_s is the sampling interval, $N_{IF}(nT_s)$ is a disturbing term and $y_{IF,i}[n]$ are the samples of the signal

$$y_{IF,i}(t) = \sqrt{2C_i}c_i\left(t-\tau_{0,i}^a\right)d_i\left(t-\tau_{0,i}^a\right)\cos\left(2\pi\left(f_{IF}+f_{d,i}^0\right)t+\varphi_i^0\right) \tag{2}$$

transmitted by the i-th satellite and received at the front-end output. C_i and $c_i\left(t-\tau_{0,i}^a\right)$ are the received power and the spreading code of the i-th satellite, $d_i\left(t-\tau_{0,i}^a\right)$ represents the bit stream of the navigation message, f_{IF} is the IF center frequency, and φ_i^0 is a random phase. Both the code and the navigation message are delayed by $\tau_{0,i}^a$; $f_{d,i}^0$ is the Doppler shift of the i-th satellite. The zero used as subscript in the parameters highlights the fact that those parameters are the ones that characterize the input signal. In (1) the quantization effect has been neglected. In the following, the notation $x[n] = x(nT_s)$ will indicate a discrete-time sequence $x[n]$, obtained by sampling a continuous-time signal $x(t)$ with a sampling frequency $f_s = \frac{1}{T_s}$.
In general the disturbing signal $N_{IF}[n] = N_{IF}(nTs)$ can be expressed as

$$N_{IF}[n] = I_{IF}[n] + W_{IF}[n] \tag{3}$$

where $I_{IF}[n]$ is, in general, a non-stationary interference and $W_{IF}[n]$ is a Gaussian noise whose spectral characteristics depend on the type of filtering and on the sampling and decimation strategy adopted in the front-end. A convenient choice is to sample the IF signal with a sampling frequency $f_s = 2B_{IF}$, where B_{IF} is the front-end bandwidth. Before sampling, an anti-aliasing low-pass filter with bandwidth $f_s/2$ is generally applied. In this case, it is easily shown that the noise variance becomes

$$\sigma_{IF}^2 = E\{W_{IF}^2(t)\} = E\{W_{IF}^2(nT_s)\} = \frac{N_0 f_s}{2} = N_0 B_{IF}$$

where $N_0/2$ is the Power Spectral Density of the IF noise. The autocorrelation function

$$R_{IF}[m] = E\{W_{IF}(nT_s)W_{IF}((n+m)T_s)\} = \sigma_{IF}^2\delta[m]$$

implies that the discrete-time random process $W_{IF}[n]$ is a classical i.i.d. (independent and identically distributed) random process, or a white sequence.

The interference $I_{IF}[n]$ is assumed to be a real mono-component signal:

$$I_{IF}[n] = A_{int}[n] \cos\left(2\pi f_{int}[n] n T_s + \varphi_I\right) \tag{4}$$

where $A_{int}[n]$ is a base-band real signal and $f_{int}[n]$ is the interference instantaneous frequency. φ_I is the interference phase, that is assumed to be a random variable uniformly distributed in the range [-π, π). The interference mean power is defined as the variance of the disturbing signal (4)

$$J = \text{Var}\left\{I_{IF}[n]\right\} \tag{5}$$

that, in case of constant amplitude signal, is equal to

$$J = \frac{A_{int}^2}{2} \tag{6}$$

The Jammer-to-Noise ratio is defined as

$$\frac{J}{N} = \frac{J}{\sigma_{IF}^2} = \frac{J}{N_0 B_{IF}} \tag{7}$$

As a result of code orthogonality the different GNSS codes are analyzed separately by the acquisition block and thus the case of a single satellite is considered hereinafter; thus the resulting signal is

$$\begin{aligned} r[n] = &\sqrt{2C} c\left[n - \tau_0\right] d\left[n - \tau_0\right] \cos\left(2\pi F_{D,0} n + \varphi^0\right) \\ &+ A_{int}[n] \cos\left(2\pi F_{int}[n] n + \varphi_I\right) + W_{IF}[n] \end{aligned} \tag{8}$$

where $F_{D,0} = \left(f_{IF} + f_d^0\right) T_s$, $F_{int} = f_{int} T_s$ and $\tau_0 = \tau_0^a / T_s$. Notice that the proposed method is valid for every value of $f_I F$ used in GNSS receivers ([14], [15]).

A. The acquisition process

In Fig. 1 the scheme of a conventional acquisition system [16] is shown: a local replica of the GNSS code, delayed of τ, and two orthogonal sinusoids at the frequency $F_D = \left(f_{IF} + f_d\right) T_s$, are generated and multiplied by the received signal $r[n]$. The resulting signals are coherently integrated, leading to the in-phase and quadrature components $S_I\left(\tau, F_D\right)$ and $S_Q\left(\tau, F_D\right)$. Those components are then squared and summed, removing the dependence from the input signal phase

φ^0. In this way a bi-dimensional function $S^2(\tau, F_D)$ is obtained. At the end the square root of this function is evaluated and used for detection purposes. In the literature $S(\tau, F_D)$ is often called *ambiguity function* [16].

When a mitigation unit is present, it is generally placed between the front-end and the subsequent

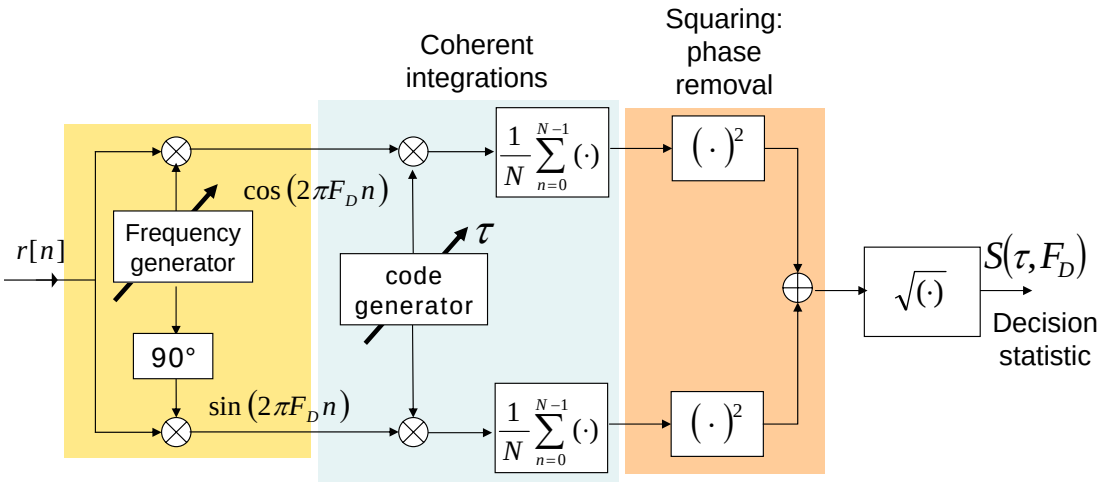

Fig. 1. Scheme of a GNSS acquisition block using coherent integrations only. The low-pass filters after the cosine/sine multiplications have been omitted, since the coherent integrations block already acts like low-pass filters

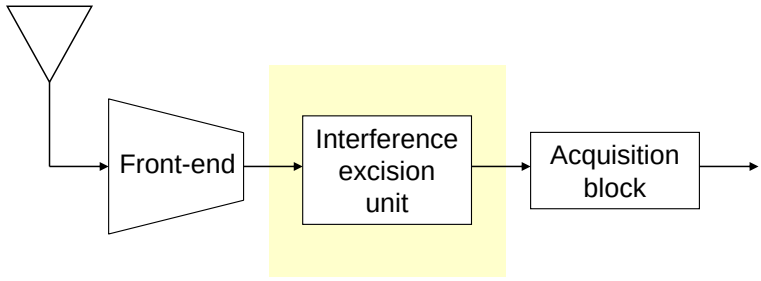

Fig. 2. Scheme of the first stages of a GNSS receiver. When an interference mitigation unit is present it is generally placed between the font-end and the subsequent stages.

stages, such as the acquisition block. In Fig. 2 the scheme of a GNSS receiver equipped with an interference unit is reported. The excision unit modifies the signal entering the acquisition block, whose performance results consequently impacted by the mitigation unit. Thus the ambiguity

function can be considered a reliable metric for assessing the validity of interference excision units.

The acquisition performance is usually evaluated by means of the Receiver Operative Characteristics (ROCs) that are the plot of the the detection versus the false alarm probability. The false alarm probability is defined under the hypothesis H_0 of signal absence or code delay/Doppler frequency mismatch as

$$P_{fa}(\beta) = P\left(S\left(\tau, F_D\right) > \beta | H_0\right) \tag{9}$$

that is the probability that the decision variable $S\left(\tau, F_D\right)$ passes a fixed threshold β under H_0. The detection probability is defined under the hypothesis H_1 of signal presence and perfect delay and frequency alignment (within the search space bin precision) between the received signal and the local replica:

$$P_{det}(\beta) = P\left(S\left(\tau_0, F_{D,0}\right) > \beta | H_1\right) \tag{10}$$

The ROCs are used in Section IV to assess the performance of our excision algorithm and to compare it with the technique proposed by [6].

III. Time-Frequency excision

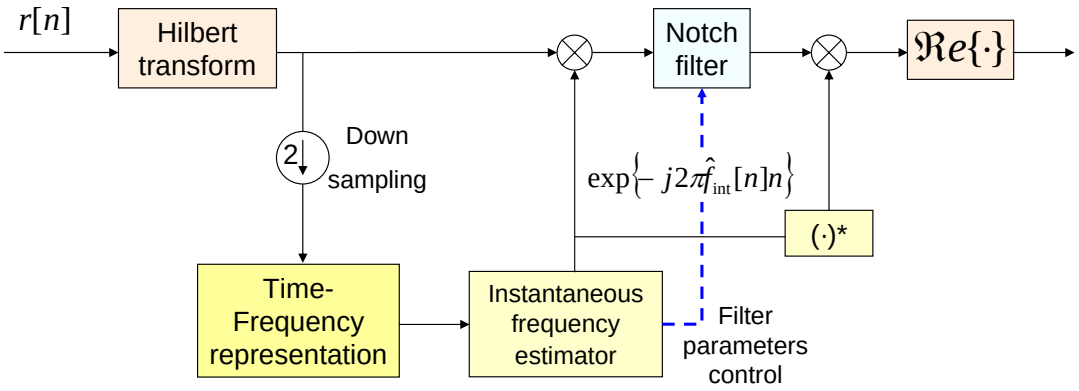

Fig. 3. Functional scheme of the TF excision algorithm. The system is essentially composed by three blocks: the TF representation, the instantaneous frequency estimation unit and the notch filter.

In this Section the description of the excision algorithm and of its functional blocks is provided. The general scheme of our interference excision unit is reported in Fig. 3. At first the analytic

representation of received signal is evaluated:

$$r_h[n] = r[n] + j\hat{r}[n] \tag{11}$$

where $\hat{r}[n]$ is the Hilbert transform of $r[n]$[17]. The analytic signal $r_h[n]$ has components belonging only to the half plane of positive frequencies and its use is necessary for avoiding the presence of cross-terms on the TF representation. These cross-terms would be generated by the interaction between positive and negative frequency components, if the real signal $r[n]$ were employed [8]. From (8) it is possible to express the analytic signal $r_h[n]$ as:

$$r_h[n] = \sqrt{2C}c_h\left[n-\tau_0\right]\exp\left\{j2\pi F_{D,0}n + j\varphi^0\right\} + A_{h,int}[n]\exp\left\{j2\pi F_{int}[n]n + j\varphi_I\right\} + W_h[n] \tag{12}$$

where $c_h\left[n-\tau_0\right]$ and $A_{h,int}[n]$ are the amplitude envelopes of the GNSS and of interference signal. In (12) the impact of the navigation message $d\left[n-\tau_0\right]$ has been neglected since its rate is usually low and thus it can be considered constant over the period used for the TF excision and the acquisition process. $W_h[n]$ is a zero mean complex gaussian noise whose real and imaginary parts are independent and have the same variance σ^2_{IF}.

Before entering the TF representation unit, $r_h[n]$ is then decimated of a factor 2 and the signal

$$r_a[n] = r_h[2n] \tag{13}$$

is obtained. This choice is justified by the fact that down-sampling $r_h[n]$ do not essentially reduce its information content [17] since the spectrum of $r_h[n]$ aliases on the negative frequencies that do not contain any signal component. In general it is desirable to deal with the lowest sampling rate consistent with the preservation of the signal information since it reduces the computational load required for the different operations. Furthermore it is possible to show that the noise component of $r_a[n]$, $W_a[n] = W_h[2n]$, has a flat spectrum over all the digital frequencies and thus it is a white sequence. This condition allows to easily evaluate the probability density function of the TF representation of $W_a[n]$ and will be used in III-B for the determination of the interference detection threshold. These considerations can be made because we assume that the front-end filter does not change the input signal spectral characteristics.

The signal $r_a[n]$ enters the TF representation unit, that allows the estimation of the interference instantaneous frequency by the subsequent unit. The estimated instantaneous frequency $\hat{f}_{int}[n]$ is employed to down-convert the interference component $A_{a,int}[n]\exp\left\{j2\pi f_{int}[n]n\right\}$ around the

zero-frequency. The jammer is then excised by a notch filter and the original frequency content is restored. At the end only the real part of the obtained signal is considered and the output signal is fed into the acquisition block.

The three functional blocks of the proposed method can be implemented by using different techniques. For example, in [6], the Wigner-Ville distribution was used as TF representation and the parameters that maximize the Hough Transform [18] of the Wigner-Ville employed for the instantaneous frequency estimation. In the next subsections these three blocks are analyzed and the algorithms developed in the context of this work discussed.

A. Time-Frequency representations

In this paper we consider two different TF representations: the spectrogram and the Wigner-Ville distribution.

The discrete time spectrogram is defined as [19]

$$Sp(n,f) = \left|\text{STFT}(n,f)\right|^2 \tag{14}$$

where $\text{STFT}(n,f)$ is the Short-Time Fourier Transform:

$$\text{STFT}(n,f) = \sum_{i=n}^{n+L-1} r_a[i]h[i-n]\exp\left\{-j2\pi if\right\} \tag{15}$$

where $h[n]$ is the analysis window of length L. The spectrogram has poor TF localization properties and its characteristics strictly depend on the analysis windows. However it requires a low computational load and is suitable for real-time applications. Moreover different strategies [20], [4] have been developed in order to select the analysis window that maximizes the localization of the interference on the TF plane.

The discrete time Wigner-Ville distribution is defined as [21]

$$W_{x,x}(n,f) = \sum_i r_a\left[n+i\right] r_a^*\left[n-i\right]\exp\left\{-j4\pi if\right\} \tag{16}$$

and does not suffer from the time versus frequency resolution tradeoff problems of the spectrogram. This property is however payed by higher computational requirements and by the possible presence of cross-terms as highlighted in the following.

Since in practice only a finite portion of the signal $r_a[n]$ is available for the evaluation of the

Wigner-Ville distribution then (16) should to be rewritten as

$$\bar{W}_{x,x}(n,f) = \sum_i r_a\left[n+i\right] w[n+i] r_a^*[n-i] w^*\left[n-i\right] \exp\left\{-j4\pi i f\right\} \tag{17}$$

where $w[n]$ is a window of finite duration that selects the portion of $r_a[n]$ available for the computation of (16).

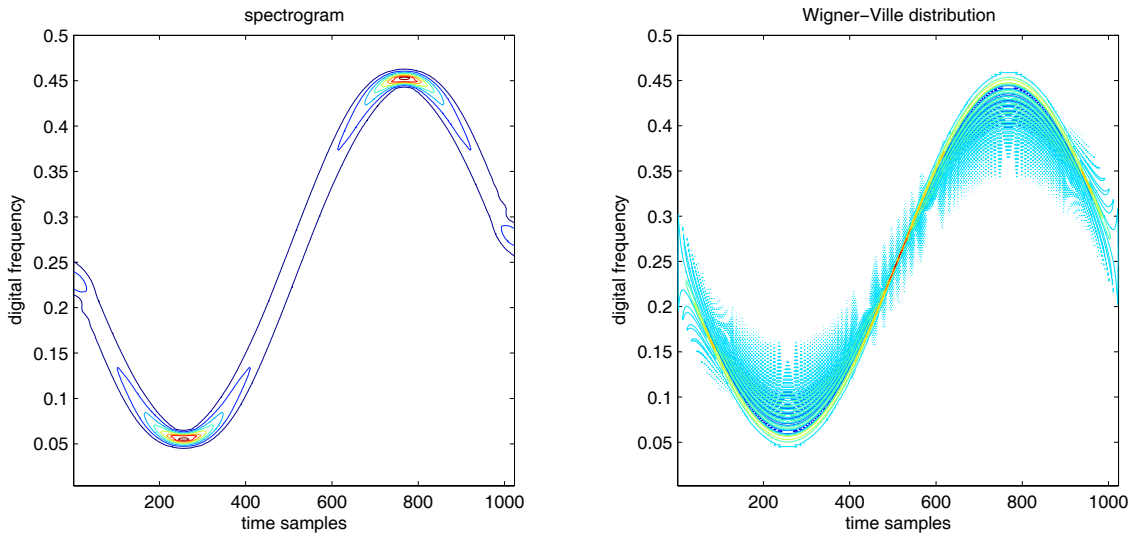

Fig. 4. Spectrogram and Wigner-Ville distribution of a signal with sinusoidal frequency modulation. The spectrogram has been evaluated by using a Hamming window of length $L = 127$ samples.

In Fig. 4 an example of spectrogram and Wigner-Ville distribution of a signal with sinusoidal frequency modulation is presented. The Wigner-Ville distribution better localizes the signal on the TF plane, even if the presence of cross-terms due to the interaction of the different signal components is more evident.

B. Instantaneous frequency (IF) estimation

A simple algorithm called peaks-interpolation is used for estimating the interference instantaneous frequency. This algorithm selects the samples of the TF representation that pass a fixed threshold and provides, as instantaneous frequency estimation, the polynomial curve that better interpolates these TF points.

The threshold for determining the TF points corrupted by the interference depends on the adopted TF representation and has been determined by fixing a false interference detection probability.

In particular, when the interference is absent and by neglecting the impact of the useful GNSS signal, it is possible to derive the probability density function of the points belonging to the TF representation. Let be TFR(n, f) the adopted TF representation, either the spectrogram (14) or the Wigner-Ville distribution (17): then the false interference detection probability is defined as

$$P_{fid}(\beta_d, n, f) = P\left(|\text{TFR}(n, f)| > \beta_d | \text{interference absent}\right) \tag{18}$$

where β_d is the interference detection threshold. From (18) it is possible to derive β_d once fixed a target false interference detection probability P_{tar}:

$$\beta_d = P_{fid}^{-1}(P_{tar}) \tag{19}$$

When the spectrogram is employed, each TF point, under the hypothesis of interference absence, is a central χ^2 random variable and the false detection probability becomes

$$P_{fid,sp}(\beta_d, n, f) = P_{fid,sp}(\beta_d) = \exp\left\{-\frac{\beta_d}{2\sigma_{IF}^2 E_h}\right\} \tag{20}$$

where E_h is the energy of the analysis window:

$$E_h = \sum_{i=0}^{L-1} h^2[i] \tag{21}$$

The proof of (20) is reported in Appendix I. In this case the threshold β_d has the following expression

$$\beta_d = -2\sigma_{IF}^2 E_h \log P_{tar} \tag{22}$$

When the TF representation is the Wigner-Ville distribution the evaluation of the probability density function of the TF points results more complex. However, since each value of (17) is obtained as the combination of several random variables, a Gaussian approximation for the probability density function is justified. Thus the false interference detection probability can be approximated by

$$P_{fid,wv}(\beta_d, n, f) = P_{fid,wv}(\beta_d, n) = \text{erfc}\left(\frac{\beta_d - \mu_{wv}}{\sqrt{2}\sigma_{wv}[n]}\right) \tag{23}$$

where $\text{erfc}(x) = \frac{2}{\sqrt{\pi}} \int_x^{+\infty} \exp\{-t^2\}\, dt$ is the complementary error function [22]. $\mu_{wv} = 2\sigma_{IF}^2$ and $\sigma_{wv}^2[n]$ are the mean and the variance of the TF points of the Wigner-Ville distribution of the input noise. The expression of $\sigma_{wv}^2[n]$ is derived in Appendix II and it is equal to

$$\sigma_{wv}^2[n] = 4\sigma_{IF}^4 \sum_i |w(n-i)|^2 |w(n+i)|^2 \tag{24}$$

From (23) the threshold β_d is determined:

$$\beta_d[n] = \sqrt{2}\sigma_{wn}[n]\text{erfc}^{-1}\left(P_{tar}\right) + \mu_{wv} \tag{25}$$

C. Excision filter

In order to effectively remove the interference signal that has been down-converted around the zero frequency, a notch filter has been used. In [6] a simple high-pass FIR filter characterized by the transfer function

$$H_b(z) = 1 - z^{-1} \tag{26}$$

has been employed. However this kind of high-pass filter introduces a wide notch that extremely degrades the useful signal quality.

This clearly emerges from Fig. 5, where the transfer function of the filter defined by (26) is

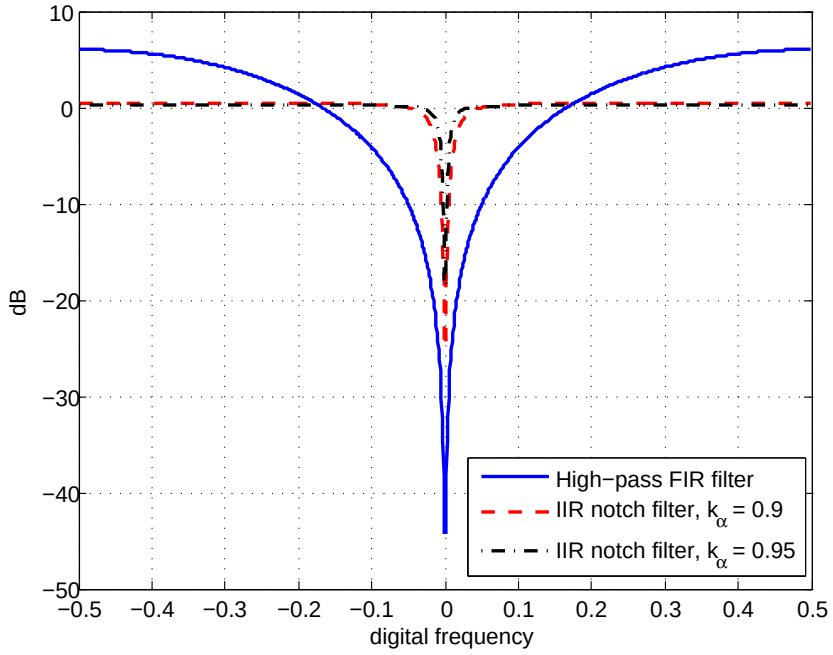

Fig. 5. Transfer functions of the different excision filters.

reported: all frequencies are distorted and the useful signal is compromised.

In order to overcome this problem we propose the use of a simple IIR notch filter defined by

$$H_c(z) = \frac{1 - z^{-1}}{1 - k_\alpha z^{-1}} \tag{27}$$

where k_α is the *pole-contraction factor*. This kind of filter presents a narrow notch and a transfer function that is almost flat in the region far from the zero frequency (Fig. 5). In this way only a slight portion of the useful signal is affected by the excision process. The 3-dB width of the notch is given by [12]:

$$B_{3dB} = \frac{|1 - k_\alpha|}{\pi} \tag{28}$$

thus the more k_α is close to unity the tightest the notch is. Notice that k_α can be regulated by the information provided by the *peaks-interpolation* algorithm. In fact the mean square error resulting from the interpolation process indicates how much the interference samples are close to the interpolating curve. A high mean square error implies that the interference is spread around the interpolating curve and consequently a wide notch is required for effectively removing the disturbing signal.

In order to highlight the effectiveness of the notch filter (27), an acquisition block like the

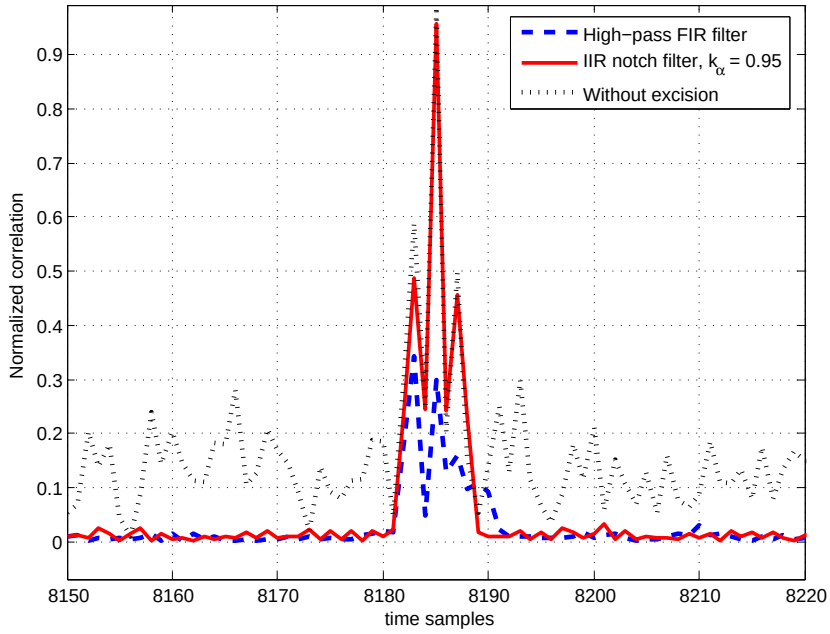

Fig. 6. Correlations of a BOC(1,1) signal in presence of interference only ($C/J = -10$dB). A linearly frequency modulated signal has been added to the GNSS signal and processed with the excision algorithm. The notch filter clearly outperforms the FIR filter proposed in [6].

one reported in Fig. 1 is considered, and three different correlations have been evaluated and

reported in Fig. 6. A linearly frequency modulated signal has been added to a BOC(1,1) signal characterized by a code of period 4092 and with a chip rate of for 4 samples per chip. The simulated signal is noise-free for better highlighting the excision filter impact on the correlation. When the mitigation unit is not present, interference makes the secondary lobes rise, potentially preventing the right detection of the correlation peak in presence of noise. When the excision unit is active the jammer is excised and the secondary lobes are clearly reduced; however, when the simple FIR filter proposed by [6] is employed, the mean correlation peak is heavily distorted and thus the IIR notch filter results preferable.

IV. Performance analysis

In this Section the performance of TF excision algorithm is analyzed. More specifically the proposed algorithm, that uses as TF representation the spectrogram and as IF estimation unit the peak-interpolation technique, is compared with the methodology developed in [6], that is based on the Wigner-Ville distribution and on the Radon-Hough transform. Different criteria are used for assessing the performance of the TF algorithm: the quality of the IF estimation is determined through its mean squared error, whereas the acquisition performance is evaluated by means of ROCs. The impact of the excision algorithm is further highlighted by comparing the ambiguity functions evaluated when the anti-jamming device is active or not.

The scenario adopted for the simulation is characterized by the parameters reported in Table I

TABLE I

Simulation parameters

Parameter	**Value**
GNSS code	GPS C/A code
Sample rate	4 samples/chip
Sampling frequency	4.092 MHz
Coherent integration time	1 ms
Intermediate frequency	38.5 KHz
Spectrogram analysis window	Hamming
Analysis window length	64 samples

and consists in a GNSS signal in zero mean Gaussian noise (with a varying C/N_0) corrupted

by a constant amplitude linearly frequency modulated interference (*chirp*). The choice of such an interference is common in the literature [6], [5] and thus it has been employed as test bench for the TF excision algorithm.

The instantaneous frequency of a chirp signal can be expressed as

$$f_{int}[n] = f_{int}^0 + a_{int}n \tag{29}$$

where f_{int}^0 is the initial interference frequency and a_{int} is the interference frequency drift. In Fig.

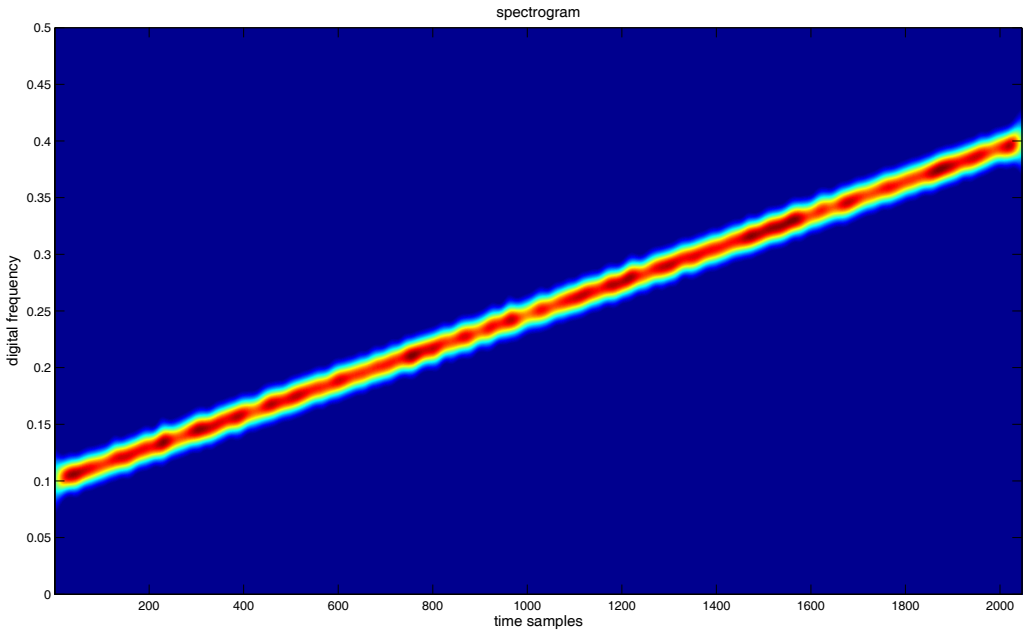

Fig. 7. Spectrogram of the simulated GPS signal in zero mean Gaussian noise and chirp interference. The disturbing signal clearly emerges from the TF plane and thus its instantaneous frequency can be easily estimated. $C/N_0 = 36$ dB-Hz, $J/N = 10$ dB.

7 the spectrogram of the signal used for simulations is depicted. The disturbing signal clearly emerges from the TF plane and thus its instantaneous frequency can be easily estimated. In Fig. 8 the Wigner-Ville distribution of the same signal is depicted. The presence of cross-terms is evident. These cross-terms emerge from the noise floor and pass the threshold defined by (25) biasing the interference frequency estimation provided by the peak-interpolation technique. For this reason the spectrogram results the best TF representation for this kind of algorithm. Conversely the Wigner-Ville distribution, thanks to its good localization properties, is more effective in conjunction with the technique based on the Radon transform.

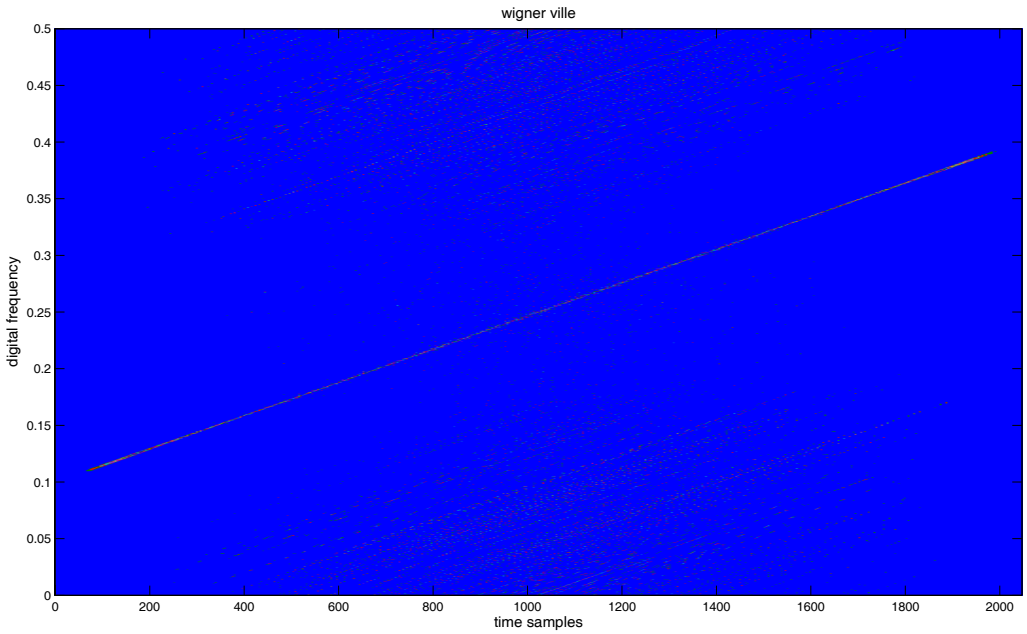

Fig. 8. Wigner-Ville distribution of the simulated GPS signal in zero mean Gaussian noise and chirp interference. The interference is well localized in the TF plane; the presence of several cross terms is also evident. $C/N_0 = 36$ dB-Hz, $J/N = 10$ dB.

A. Interference detection

In order to detect the interference presence, the thresholds defined by (22) and (25) are applied to the spectrogram of Fig. (7) and to the Wigner-Ville distribution of Fig. (8) respectively. This process leads to the detection of the samples highlighted in Fig.s 9 and 10. In both cases the target false interference detection probability P_{tar} has been set to 10^{-7}, that is less than the inverse of the number of samples of the TF representation. This is a rule-of-thumb adopted in order to prevent that a sample of the TF representation accidently passes the threshold even if not affected by the interference. Fig.s 9 and 10 show the effectiveness of the threshold evaluated in Section III-B, since only the samples affected by the interference are correctly detected. Even if the Wigner-Ville distribution does not result effective in conjunction with the peak-interpolation technique, the threshold (25) can be used for interference detection and for other applications, such as TF masking, since till now the decision threshold was only empirically set [9].

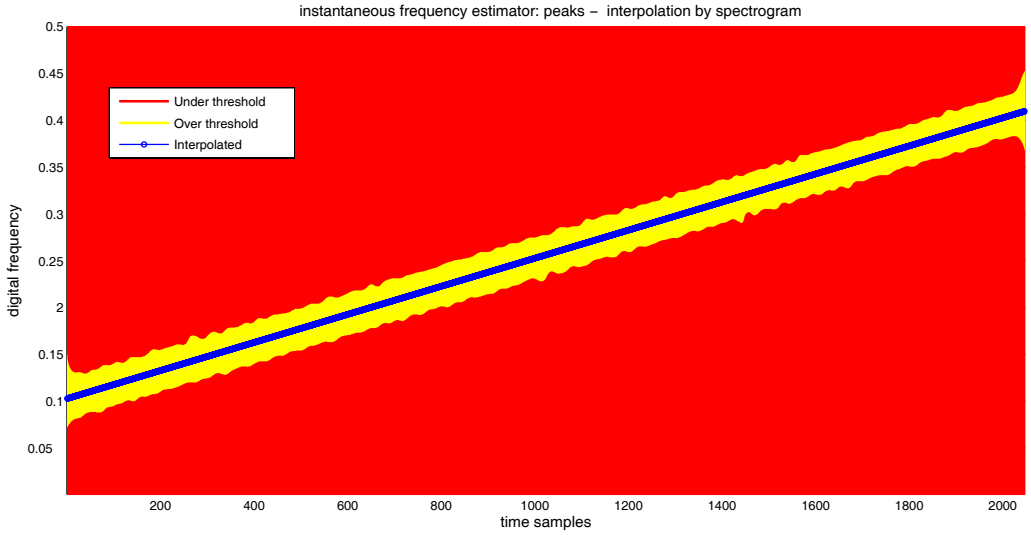

Fig. 9. Interference detection: those samples of the spectrogram that pass the decision threshold are declared corrupted by the disturbing signal. These samples (light zone) are interpolated by the peak-interpolator unit, that determines the instantaneous frequency $f_{int}[n]$.

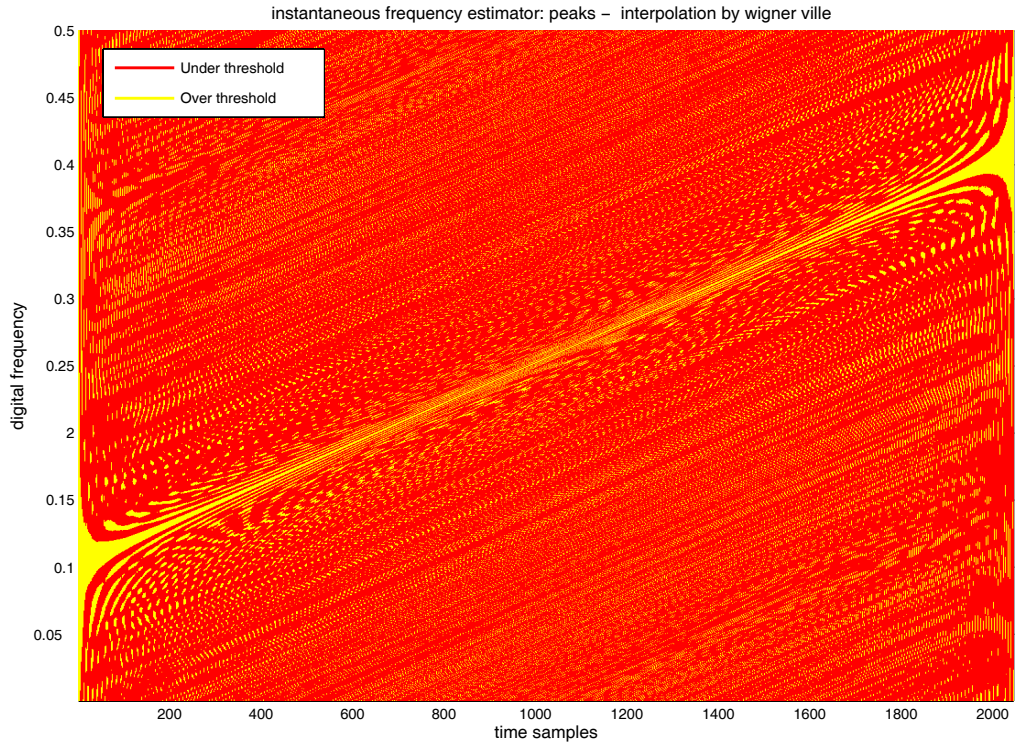

Fig. 10. Interference detection: those samples of the Wigner-Ville distribution that pass the decision threshold are declared corrupted by the disturbing signal. The presence of cross-terms biases the instantaneous frequency estimation.

B. *Peak-interpolation performance*

The peak-interpolation technique estimates the parameters that define the interference IF as

$$\left[f_{int}^{0}; a_{int}\right] = \arg\min_{f,a} \left\| \vec{Y} - f - a\vec{X} \right\|^2 \tag{30}$$

where $\vec{Y}$ and $\vec{X}$ are the vectors of the TF coordinates of the samples that pass the detection threshold. In Fig. 9 the frequency estimation provided by the peak-interpolation has been superimposed to those samples that pass the threshold in the spectrogram: the estimation almost agrees with the true frequency proving the effectiveness of the algorithm. In Fig. 11 the mean squared

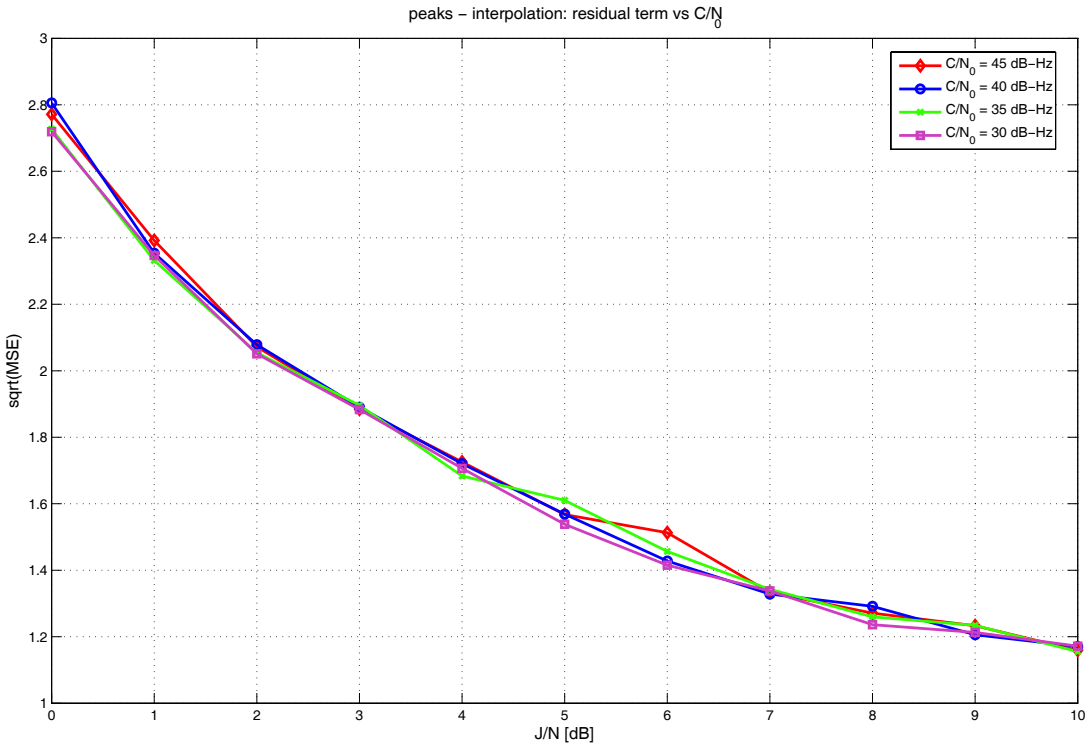

Fig. 11. Mean squared error of the interference frequency estimation provided by the peak-interpolation algorithm vs. the Jammer to Noise ratio.

error of the interference frequency estimation provided by the peak-interpolation algorithm is depicted as function of the Jammer to Noise ratio (J/N). The error is less than a few Hertz also for low J/N and decreases as the J/N increase. Three different C/N_0s have been considered, however the impact of the GNSS signal on the estimation process is only marginal and the peak-interpolation error is almost constant with respect to the C/N_0.

C. ROC

In order to test the behavior of the excision unit, and in particular the impact of an IIR filter, ROCs under different working conditions have been evaluated by Monte Carlo simulations. In Fig. 12 the true interference frequency has been used to down-convert the disturbing signal. As

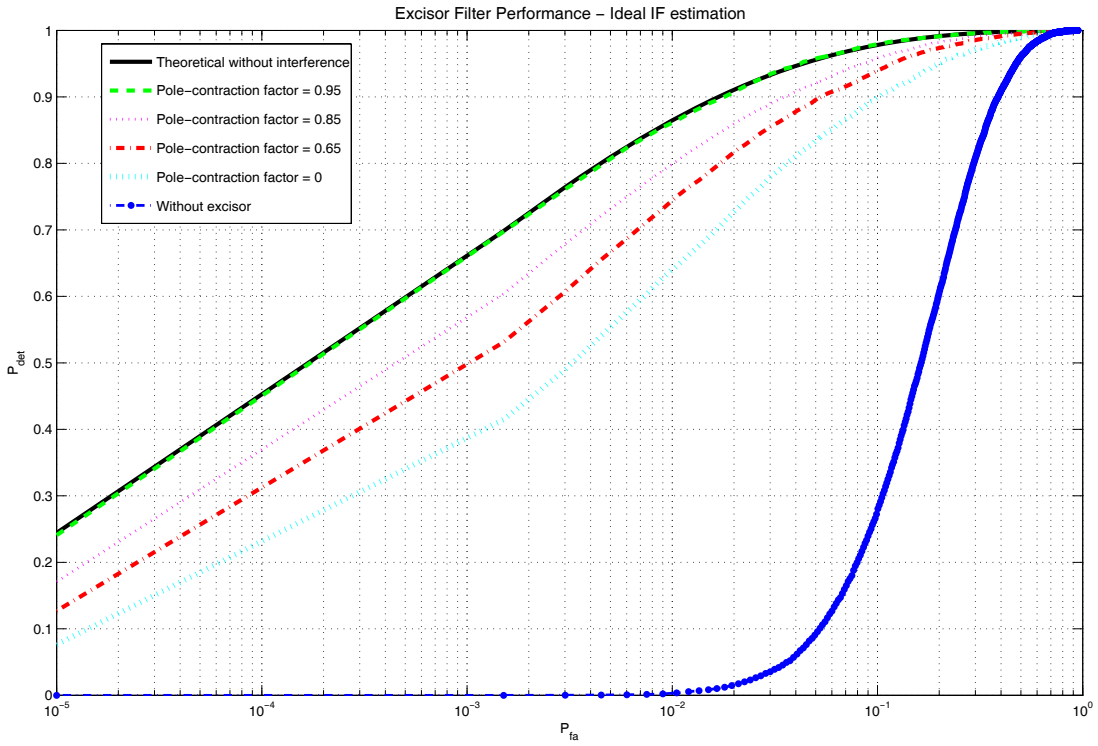

Fig. 12. ROC curves for different pole contraction factors with an ideal IF estimation. $C/N_0 = 36$ dB-Hz, $J/N = 10$ dB.

expected the presence of an excision unit extremely increases the system performance. Moreover, the more k_α, the pole-contraction factor, approaches unity, the more the performance is close to the ideal one, that is in absence of interference. The performance obtained by using the FIR filter proposed by [6] ($k_\alpha = 0$) results clearly worse than the ones achievable by employing the IIR filter (27). This proves that the use of notch IIR filters extremely increases the acquisition performance and that the GNSS signal is not essentially impacted by the correlation introduced by this kind of filters. In Fig. 13 the interference IF has been recovered by using either the peak-interpolation technique in conjunction with the spectrogram or the Radon transform in conjunction with the Wigner-Ville distribution[6]. Both estimation techniques cause a slight

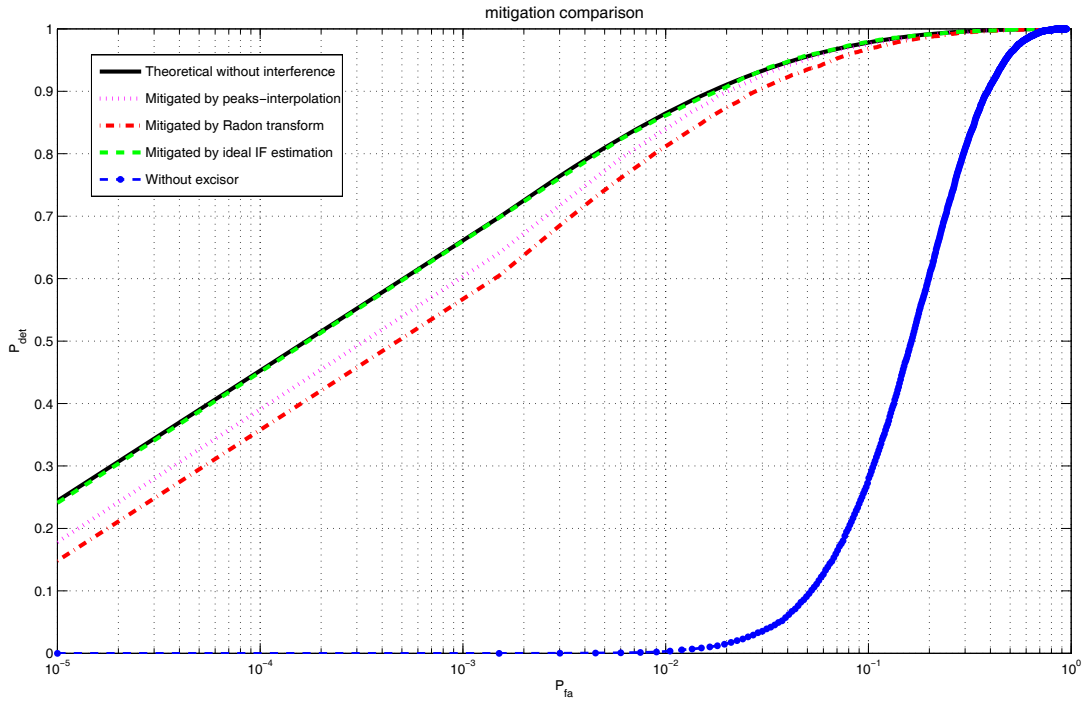

Fig. 13. ROC curves for different IF estimation techniques. $C/N_0 = 36$ dB-Hz, $J/N = 10$ dB, $k_\alpha = 0.95$.

degradation of the ROCs, however, in the case analyzed in Fig. 13, the peak-interpolation algorithm provides a better performance.

D. Impact on the ambiguity function

Finally, in Fig. 14, the impact of our excision unit on the ambiguity function is shown. In this case an excision filter with $k_\alpha = 0.95$ has been used and the interference frequency has been estimated by using the peak-interpolation technique. When the excision unit is active the jammer is effectively removed and the signal peak clearly emerges from the noise floor of the ambiguity function, allowing a correct signal acquisition.

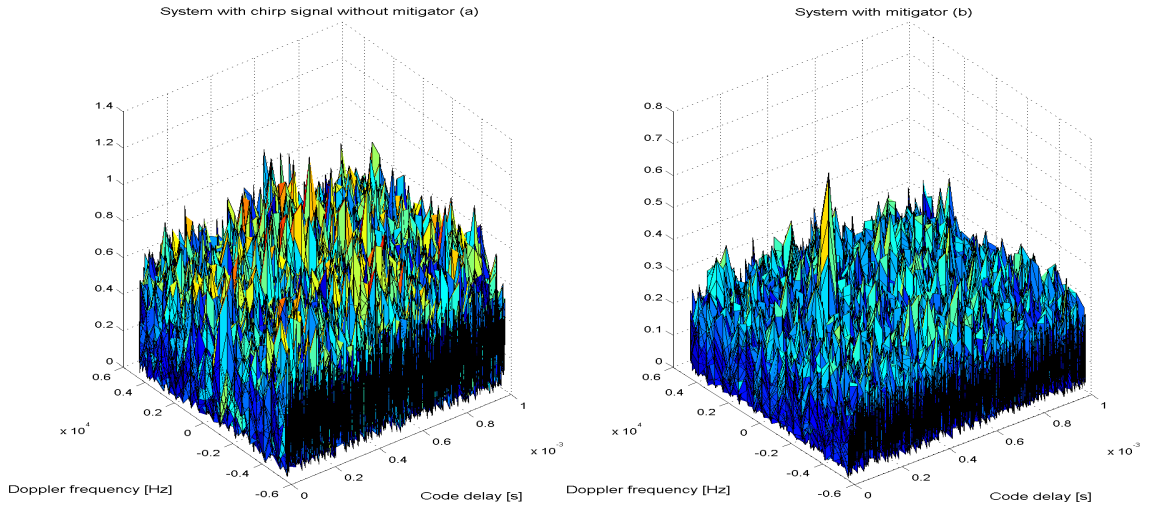

Fig. 14. Comparison between ambiguity functions of a GPS signal affected by chirp interference. $C/N_0 = 45$ dB-Hz, $J/N = 10$ dB. a) Without excision unit; b) with excision unit.

V. Conclusions

In this paper a novel Time-Frequency algorithm for interference excision for GNSS applications has been developed. We showed that a general class of TF excision algorithms can be represented by three functional blocks: the TF representation, the interference IF estimation unit and the excision filter. In this context we proposed the use of the spectrogram, for its low computational requirements with respect to other TF representations, and of a simple interpolation technique for the IF estimation. An interference detection system, based on the statistical properties of TF representations has been also proposed and an analytical expression for the interference detection threshold has been derived. Moreover the use of IIR notch filters for interference excision has been introduced.

The proposed method is effective and outperforms past algorithms already present in the literature.

Appendix I

Probability density function of the spectrogram of Gaussian white noise

In this Appendix we show that each point of the spectrogram of white gaussian noise is χ^2 or equivalently exponentially distributed. The input noise is supposed zero mean with independent

and identically distributed (i.i.d) real and imaginary parts of variance σ_{IF}^2.

It is well known [23] that the square absolute value of a zero mean complex Gaussian random variable, with independent real and imaginary parts, is χ^2 distributed, with parameter equal to the variance of the initial complex Gaussian random variable. Thus we have to show that the STFT(n,f) is a complex Gaussian random variable, determine its variance and prove the independence between its real and imaginary parts. STFT(n,f) is Gaussian and zero mean since it is a linear combination of zero mean Gaussian random variables. The variance of STFT(n,f) is given by

$$\begin{aligned}\text{Var}\left\{\text{STFT}(n,f)\right\} &= \text{E}\left[|\text{STFT}(n,f)|^2\right] \\ &= \text{E}\left[\sum_i r_a[i]h[i-n]\exp\{-j2\pi if\}\sum_l r_a^*[l]h^*[l-n]\exp\{j2\pi lf\}\right] \\ &= \sum_i\sum_l \text{E}\left[r_a[i]r_a^*[l]\right]h[i-n]h^*[l-n]\exp\{-j2\pi(i-l)f\}\end{aligned} \tag{31}$$

Since $r_a[n]$ is white and zero mean, the only terms that survive in the summation in (31) are those corresponding to $i=l$. Thus (31) becomes

$$\begin{aligned}\text{Var}\left\{\text{STFT}(n,f)\right\} &= \sum_i \text{E}\left[|r_a[i]|^2\right]|h[i-n]|^2 \\ &= 2\sigma_{IF}^2\sum_i |h[i-n]|^2 = 2\sigma_{IF}^2 E_h\end{aligned} \tag{32}$$

where $E_h=\sum_i |h[i-n]|^2$ is the energy of the analysis window.

In order to prove the independence between real and imaginary parts of STFT(n,f) it is enough to show that the covariance $\text{E}\left[\mathbb{R}e\left\{\text{STFT}(n,f)\right\}\mathbb{I}m\left\{\text{STFT}(n,f)\right\}\right]$ is equal to zero. In particular:

$$\begin{aligned}&\text{E}\left[\mathbb{R}e\left\{\text{STFT}(n,f)\right\}\mathbb{I}m\left\{\text{STFT}(n,f)\right\}\right] \\ &= \text{E}\left[\sum_i \mathbb{R}e\left\{r_a[i]h[i-n]\exp\{-j2\pi if\}\right\}\sum_l \mathbb{I}m\left\{r_a[l]h[l-n]\exp\{-j2\pi lf\}\right\}\right] \\ &= \sum_i\sum_l \text{E}\left[\mathbb{R}e\left\{r_a[i]\exp\{-j2\pi if\}\right\}\mathbb{I}m\left\{r_a[l]\exp\{-j2\pi lf\}\right\}\right]h[i-n]h[l-n] \\ &= \sum_i \text{E}\left[\mathbb{R}e\left\{r_a[i]\exp\{-j2\pi if\}\right\}\mathbb{I}m\left\{r_a[i]\exp\{-j2\pi if\}\right\}\right]h^2[i-n]\end{aligned} \tag{33}$$

where the fact that $r_a[n]$ is a white zero-mean sequence has been used to obtain the last expression in (33). The term $\mathrm{E}\left[\mathbb{R}e\left\{r_a[i]\exp\{-j2\pi if\}\right\}\mathbb{I}m\left\{r_a[i]\exp\{-j2\pi if\}\right\}\right]$ is equal to

$$\begin{aligned}
&\mathrm{E}\left[\mathbb{R}e\left\{r_a[i]\exp\{-j2\pi if\}\right\}\mathbb{I}m\left\{r_a[i]\exp\{-j2\pi if\}\right\}\right]\\
&=\mathrm{E}\left[(r_R[i]\cos(2\pi if)+r_I[i]\sin(2\pi if))(-r_R[i]\sin(2\pi if)+r_I[i]\cos(2\pi if))\right]\\
&=\mathrm{E}\left[-r_R^2[i]\cos(2\pi if)\sin(2\pi if)+r_I^2[i]\cos(2\pi if)\sin(2\pi if)+r_R[i]r_I[i](\cos^2(2\pi if)-\sin^2(2\pi if))\right]\\
&=\frac{1}{2}\sin(4\pi if)\mathrm{E}\left[r_I^2[i]-r_R^2[i]\right]=0
\end{aligned} \tag{34}$$

where $r_R[i]$ and $r_I[i]$ are the real and imaginary parts of $r_a[i]$. Eq. (34) is equal to zero since $r_R[i]$ and $r_I[i]$ are supposed independent and identically distributed. From (34) it results that the covariance between the real and imaginary parts of the STFT is zero, and thus these two components are independent. Therefore $Sp(n,f) = |\mathrm{STFT}(n,f)|^2$ is χ^2 distributed and the probability $P(|Sp(n,f)| > \beta_d) = P(Sp(n,f) > \beta_d)$ is equal to [23]:

$$P(|Sp(n,f)| > \beta_d) = P(Sp(n,f) > \beta_d) = \exp\left\{-\frac{\beta_d}{2\sigma_{IF}^2 E_h}\right\} \tag{35}$$

APPENDIX II
MEAN AND VARIANCE OF THE WIGNER-VILLE DISTRIBUTION OF GAUSSIAN WHITE NOISE

In this Appendix we evaluate the mean and variance of the Wigner-Ville distribution (17) of a complex Gaussian white noise. The noise is supposed zero mean with i.i.d. real and imaginary parts of variance σ_{IF}^2.

The mean is given by

$$\mu_{wv} = \mathrm{E}\left\{\bar{W}_{x,x}(n,f)\right\} = \mathrm{E}\left\{\sum_i r_a\left[n+i\right]w[n+i]r_a^*[n-i]w^*\left[n-i\right]\exp\left\{-j4\pi if\right\}\right\} \tag{36}$$

Since $r_a[i]$ is a white, zero-mean sequence the only non-null contribution in the summation of (36) is for $i=0$, and thus μ_{wv} is equal to

$$\mu_{wv} = \mathrm{E}\left\{|r_a[n]|^2\right\}|w[n]|^2 = 2\sigma_{IF}^2|w[n]|^2 \tag{37}$$

If $w[n]$ is a rectangular window then $|w[n]|^2 = 1$ for each n for which the Wigner-Ville distribution is defined and $\mu_{wv} = 2\sigma_{IF}^2$.

In the same way it is possible to evaluate the variance of $\bar{W}_{x,x}(n,f)$ as

$$\mathrm{Var}\left[\bar{W}_{x,x}(n,f)\right] = \mathrm{E}\left[|\bar{W}_{x,x}(n,f)|^2\right] - \left|\mathrm{E}\left[\bar{W}_{x,x}(n,f)\right]\right|^2 \tag{38}$$

The second central moment of $\bar{W}_{x,x}(n,f)$ is given by:

$$\mathrm{E}\left[|\bar{W}_{x,x}(n,f)|^2\right] =$$
$$= \sum_i \sum_l \mathrm{E}\left\{r_a[n+i]r_a^*[n-i]r_a^*[n+l]r_a[n-l]\right\} w[n+i]w^*[n-i]w^*[n+l]w[n-l]\exp\left\{-j4\pi(i-l)f\right\} \tag{39}$$

The only terms that give a non-zero contribution in (39) are those corresponding to $l=i$, and thus the second central moment of $\bar{W}_{x,x}(n,f)$ becomes

$$\begin{aligned}
\mathrm{E}\left[|\bar{W}_{x,x}(n,f)|^2\right] &= \sum_i \mathrm{E}\left\{|r_a[n+i]|^2|r_a[n-i]|^2\right\}|w[n+i]|^2|w[n-i]|^2 \\
&= \sum_{i\neq 0} \mathrm{E}\left\{|r_a[n+i]|^2\right\}\mathrm{E}\left\{|r_a[n-i]|^2\right\}|w[n+i]|^2|w[n-i]|^2 + \mathrm{E}\left\{|r_a[n]|^4\right\}|w[n]|^4 \\
&= 4\sigma_{IF}^4 \sum_{i\neq 0}|w[n+i]|^2|w[n-i]|^2 + 8\sigma_{IF}^4|w[n]|^4 \\
&= 4\sigma_{IF}^4 \sum_{i}|w[n+i]|^2|w[n-i]|^2 + 4\sigma_{IF}^4|w[n]|^4
\end{aligned} \tag{40}$$

In (40) the property that the fourth moment of a zero mean complex Gaussian random variable with i.i.d real and imaginary parts is equal to $8\sigma_{IF}^4$ has been used. Finally from (40) and (37) it is possible to evaluate

$$\mathrm{Var}\left[\bar{W}_{x,x}(n,f)\right] = 4\sigma_{IF}^4 \sum_i |w[n+i]|^2|w[n-i]|^2 \tag{41}$$

REFERENCES

[1] R. J. Landry and A. Renard, "Analysis of potential interference sources and assessment of present solutions for GPS/GNSS receivers," *4th Saint-Petersburg on INS*, May 1997.

[2] M. V. Tazebay and A. N. Akansu, "A performance analysis of interference excision techniques in direct sequence spread spectrum communications," *IEEE Trans. Signal Processing*, vol. 46, no. 9, pp. 2530 – 2535, Sep. 1998.

[3] C. Wang and M. G. Amin, "Performance analysis of instantaneous frequency-based interference excision techniques in spread spectrum communications," *IEEE Trans. Signal Processing*, vol. 46, no. 1, pp. 70 – 82, Jan. 1998.

[4] M. G. Amin, C. Wang, and A. R. Lindsey, "Optimum interference excision in spread spectrum communications using open-loop adaptive filters," *IEEE Trans. Signal Processing*, vol. 47, no. 7, pp. 1966 – 1976, Jul. 1999.

[5] X. Ouyang and M. G. Amin, "Short-time fourier transform receiver for nonstationary interference excision in direct sequence spread spectrum communications," *IEEE Trans. Signal Processing*, vol. 49, no. 4, pp. 851 – 863, Apr. 2001.

[6] S. Barbarossa and A. Scaglione, "Adaptive time-varying cancellation of wideband interferences in spread-spectrum communications based on timefrequency distributions," *IEEE Trans. Signal Processing*, vol. 47, no. 4, pp. 957 – 965, Apr. 1999.

[7] S. R. Lach, M. G. Amin, and A. R. Lindsey, "Broadband interference excision for software-radio spread-spectrum communications using timefrequency distribution synthesis," *IEEE J. Select. Areas Commun.*, vol. 17, no. 4, pp. 704 – 714, Apr. 1999.

[8] L. Cohen, *Time Frequency Analysis: Theory and Applications*. Prentice Hall PTR, Dec. 1994.

[9] Z. Yimin, M. Amin, and A. Lindsey, "Anti-jamming GPS receivers based on bilinear signal distributions," *In Proc. of Military Communications Conference (MILCOM)*, vol. 2, pp. 1070 – 1074, Oct. 2001.

[10] R. Landry, V. Calmettes, and M. Bousquet, "Impact of interference on a generic GPS receiver and assessment of mitigation techniques," *in Proc. of IEEE 5th International Symposium on Spread Spectrum Techniques and Applications*, vol. 1, pp. 87 – 91, Sep. 1998.

[11] M. Wann-Jiun, M. Wei-Lung, and C. Fan-Ren, "Design of adaptive all-pass based notch filter for narrowband anti-jamming GPS system," *in Proc. of International Symposium on Intelligent Signal Processing and Communication Systems (ISPACS)*, pp. 305 – 308, Dec. 2005.

[12] D. Borio, L. Camoriano, L. L. Presti, and P. Mulassano, "Analysis of the one-pole notch filter for interference mitigation: Wiener solution and loss estimations," in *in Proc. of ION/GNSS*, Fort Worth, TX, 2006.

[13] E. D. Kaplan and C. Hegarty, Eds., *Understanding GPS: Principles and Applications*, 2nd ed. Artech House Publishers, Nov. 2005.

[14] W.Zhuang and J. Tranquilla, "Digital baseband processor for the GPS receiver (parts I and II)," *IEEE Trans. Aerosp. Electron. Syst.*, vol. 29, pp. 1343 – 1349, Oct. 1993.

[15] J. Bao and Y. Tsui, *Fundamentals of Global Positioning System Receivers, a software approach*, 2nd ed. John Wiley and Sons, Inc, 2005.

[16] P. Misra and P. Enge, *Global Positioning System: Signals, Measurements and Performance*. Ganga Jumuna Press, 2006.

[17] S. L. Marple Jr., "Computing the discrete-time 'analytic' signal via fft," *IEEE Trans. Signal Processing*, vol. 47, no. 1999, pp. 2600–2603, Sep. 9.

[18] D. Ballard, "Generalizing the hough transform to detect arbitrary shapes," *Pattern Recognit.*, vol. 13, no. 2, pp. 111 – 122, 1981.

[19] J. B. Allen and L. R. Rabiner, "A unified approach to short-time fourier analysis and synthesis," *Proc. IEEE*, vol. 65, no. 11, pp. 1558 – 1564, Nov. 1977.

[20] M. Amin and K. D. Feng, "Short-time fourier transforms using cascade filter structures," *IEEE Trans. Circuits Syst. II*, vol. 42, no. 10, pp. 631 – 641, Oct. 1995.

[21] B. Boashash and P. J. Black, "An efficient real-time implementation of the wigner-ville distribution," *IEEE Trans. Acoust., Speech, Signal Processing*, vol. 35, no. 1, pp. 1611 – 1618, Nov. 1987.

[22] M. Abramowitz and I. A. Stegun, Eds., *Handbook of Mathematical Functions: with Formulas, Graphs, and Mathematical Tables*. Dover Publications, Jun. 1965.

[23] J. Proakis, *Digital Communications*, 4th ed. McGraw-Hill Science/Engineering/Math, Aug. 2000.